

Analysis of the HST Thermal Background as Seen by NICMOS + NCS

M. Sosey, T. Wheeler, A. Sivaramakrishnan
May 14, 2003

ABSTRACT

This report describes the results from the SMOV3b and Cycle 11 thermal background calibration programs for NICMOS. The HST aft shroud is warmer due to ongoing degradation of the external MLI and increased power of the instruments installed during SM3B (ACS and the Nicmos Cooling System (NCS)). This warms the NICMOS fore-optics, affecting the thermal background in long wavelength camera 2 and camera 3 filters by approximately 20% beyond the increase due to DQE alone. This should be taken into account when planning observations with these cameras in filters longward of 1.9 microns, or in especially broad filters such as F175W in camera 3. Since camera 1 has no filters with a central wavelength longward of 1.9 microns, thermal emission effects in this camera are not an issue, and have not been studied.

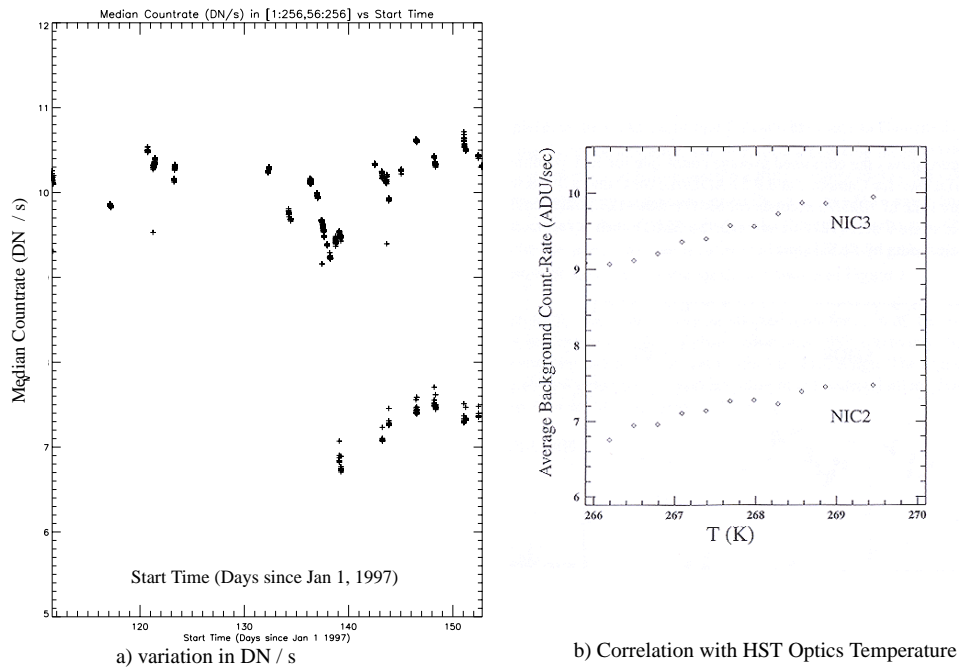
Introduction

During the 4th Hubble Servicing mission (SM3B) the NICMOS CryoCooling System was installed on the spacecraft to cool the NICMOS detectors and re-enable science observations. A radiator was attached to the +V2 side of the aft shroud to dissipate the heat extracted from the instrument and the cryocooler itself. Heat is removed from inside the aft shroud of the telescope to the external radiator by means of the Capillary Pump Loop (CPL). This is a two-phase heat transfer system that circulates ammonia by capillary action. Neon gas is circulated between the cooling system and the inside of the NICMOS

Cryostat to cool the detectors. More detailed information on the operation of the NCS can be found in Chapter 2 of the NICMOS Instrument Handbook.

Previous analysis from the pointed thermal background calibration program in Cycle 7 (7047) revealed that the HST thermal emission was overall fairly stable, and did not vary with respect to observation time, large telescope slews, and telescope pointing (Daou & Skinner 1997). Parallel science observations (program 7048) in cameras 2 and 3 were taken at different pointings in order to determine the orbital and secular variations of the thermal background seen by NICMOS. It was found that the HST thermal background was stable to within 5% over orbital time scales and to within 8% over secular time scales, regardless of which instrument was designated as prime (Daou & Calzetti 1998). It also correlated the observed secular variations (see Figure 1 a) with the temperature of the HST optics (see Figure 1 b).

Figure 1: Cycle 7 - Correlation of background variation with HST optics temperature



Calibration program 9269, and subsequently 9702 for the camera 2 images, was crafted to mimic the observations from the parallel program in Cycle 7 to assess any changes in the thermal background for Cycle 11 and beyond.

Analysis

Comparison of Cycle 7/7n and Cycle 11 datasets

Parallel observations were crafted for camera 3, in the F222M filter to re-measure the average thermal background seen by NICMOS for Cycles 11 and beyond. Taking into account the increase in detector quantum efficiency at the higher operating temperature of

77.1K, the measured thermal background was predicted from the increase in DQE to be approximately 20% higher than that during Cycle 7 for F222M. Table 1 compares the observed and predicted values from all cycles. On average, the increase in thermal background is approximately another 20% above the predicted change for Cycle 11.

Table 1. Comparison of observed and predicted thermal background values. All values for the thermal background are represented as the mean of the available datasets

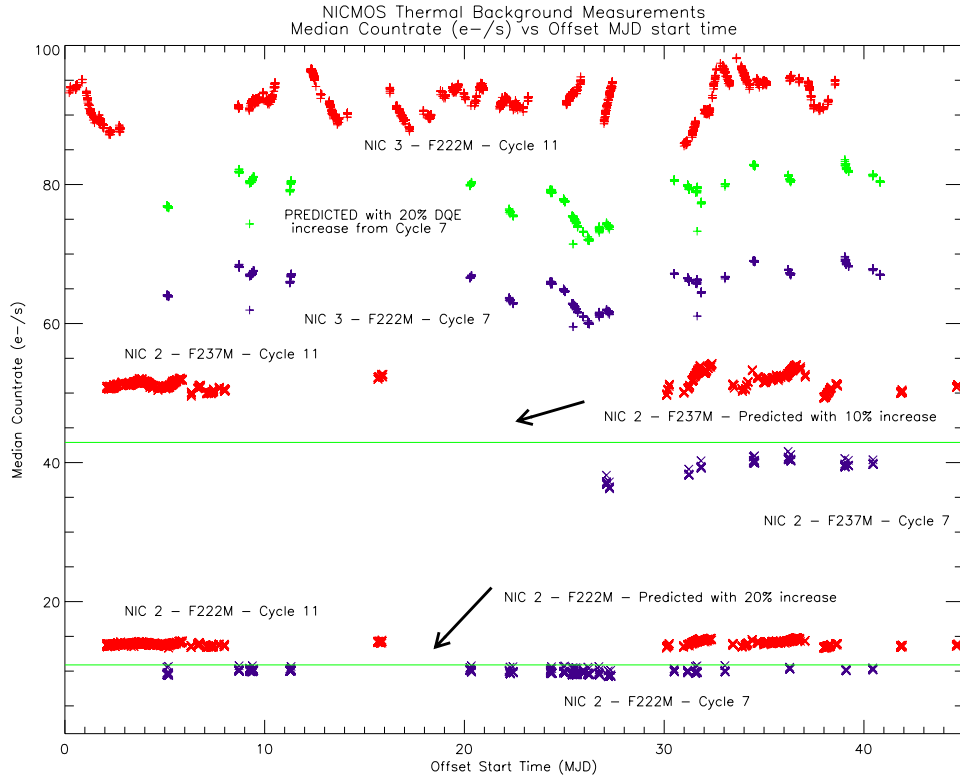
Cam	Filter	Cycle 7/7n		Cycle 11				
		Observed		Observed		Predicted		
		(DN / s)	(e- / s / pixel)	(DN / s)	(e- / s / pixel)	(DN / s)	(e- / s / pixel)	DQE increase for filter (Cycle 11)
2	F222M	1.83	9.89	2.57	13.88	2.02	10.89	21%
2	F237M	7.30	39.41	9.46	51.06	7.94	42.90	10%
3	F222M	10.06	65.36	14.18	92.16	12.07	78.44	20%

Table 1 is represented in graphical form in Figure 2. This graph better shows the difference between the predicted increase in thermal background in Cycle 11 over that actually measured from on-orbit datasets. The most noticeable difference is in camera 3, whose long wavelength F222M filter sees the most variable change in the thermal background - with peak-to-peak variations of 14% (Cycle 11). Similar variation was seen in the Cycle 7/7n data, which had a peak-to-valley range of ~ 15%. The camera 2 thermal background is also variable, although to a smaller extent.

Camera 2 datasets show increasing thermal background with wavelength - the F237M background has more pronounced variations than the F222M filter, but both still appear to see less thermal background in general than camera 3. This is due to the difference in pixel scale between the two cameras. Camera 2 has a pixel scale of 0.075 mas while camera 3's pixel scale is 0.2 mas - translating to ω , the solid angle that a detector pixel subtends on the sky - camera 2: $\omega = 5.29 \cdot 10^{-13} \text{ m}^2 / \text{sterradian}$, camera 3: $\omega = 3.61 \cdot 10^{-12} \text{ m}^2 / \text{sterradian}$. This scales to a factor of approximately 6.8 between the cameras, which makes up the difference between the median camera 2 F222M observed thermal background and that from camera 3 F222M ($13.88 \text{ e- / s / pixel} * 6.8 \sim 93 \text{ e- / s / pixel}$). Figure 3 is a plot showing this comparison using the actual data.

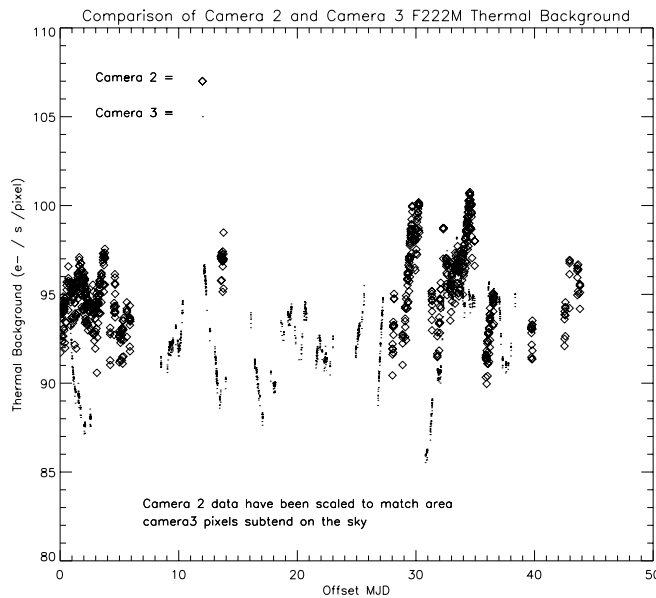
It should be noted that all values presented in this paper are in count rates, but that the exposure times for all the images being compared are 127.96 seconds. Also, temperature sensor measurements are reported in the units they are recorded (either Kelvins or Celsius). In general, temperatures inside NICMOS are reported in Kelvins, while those outside are reported in Celsius (all temperature comparisons involving measured NICMOS datasets were done in Kelvins).

Figure 2: Comparison of available thermal background data



In the figure above, solid lines are associated with the camera 2 predicted thermal background levels based on the available Cycle 7 datasets. Camera 3 predictions were also predicted using the available Cycle7 datasets, but because the emission is much more variable, no median background emission was assumed for the prediction.

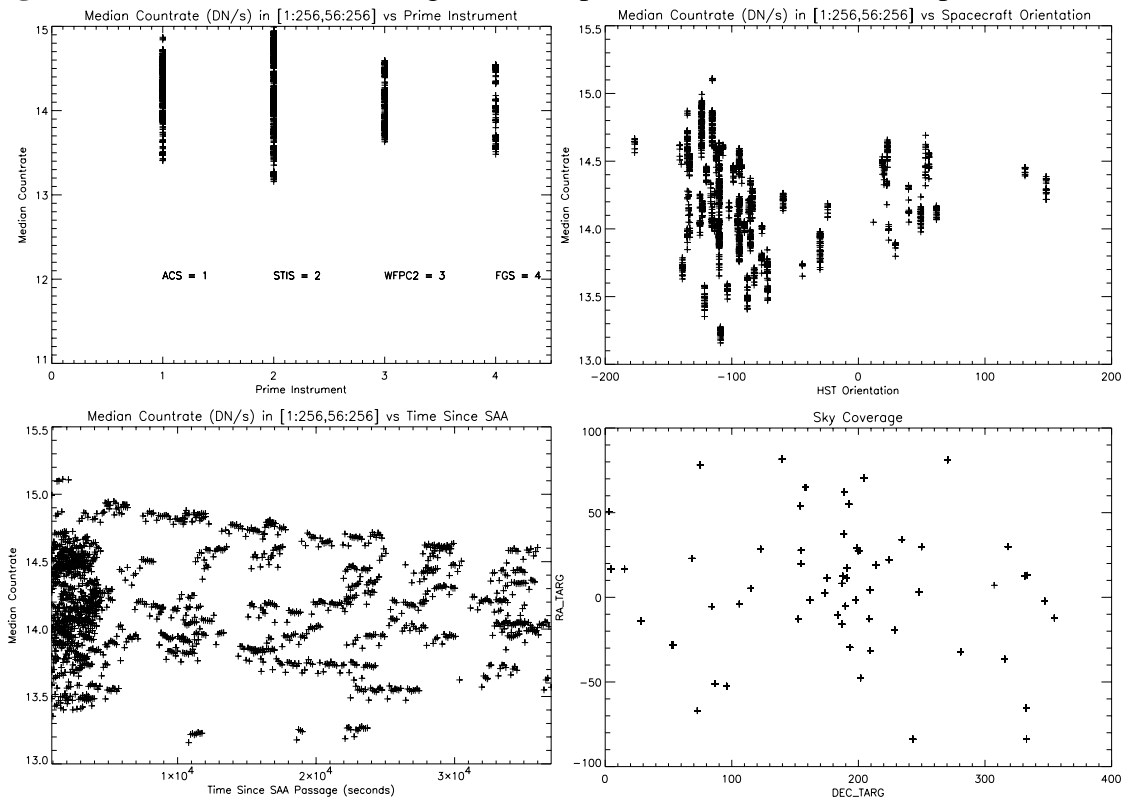
Figure 3: Comparison of F222M between NIC2 and NIC3 Thermal Background



Analysis of the Cycle 11 data

In an effort to ascertain the cause of the increased thermal flux, all available observational parameters were investigated. No correlation was found between the variation in the thermal background and telescope pointing, sun angle, prime instrument, time since the SAA passage or spacecraft orientation. However, a larger spread in measured thermal background values was observed for orientations that were highly negative (orientation taken from ORIENTAT keyword). This is a position angle measured in degrees from North through East to the positive direction of the y-axis of the Science Instrument Corrected System (SICS) of the science aperture specified in APEROBJ). A small downward slope in the measured thermal background can be seen in datasets taken further away from an SAA passage, however, the scatter of the measurements makes this relatively insignificant (see Figure 4).

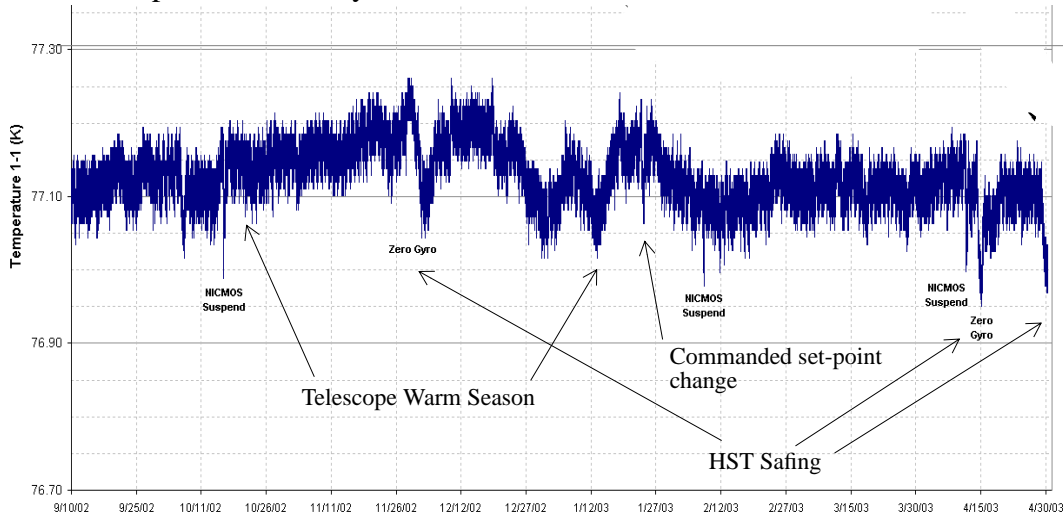
Figure 4: Camera 3 thermal background comparisons with observational parameters



Next, all pertinent temperature sensors were investigated to ascertain the thermal operating environment of the instrument and assess any changes. The only internal sensor which is useful for obtaining the temperature of the detectors themselves is the T-1-1 Mounting Cup Sensor (NDWTMP11). T-1-3 is the closest in proximity to camera 3 and was used during previous cycles. However, it has a measurement limit of 76.28 K, lower

than the current operating temperature of 77.1K, so the T-1-1 sensor is used for all cameras during Cycle 11.

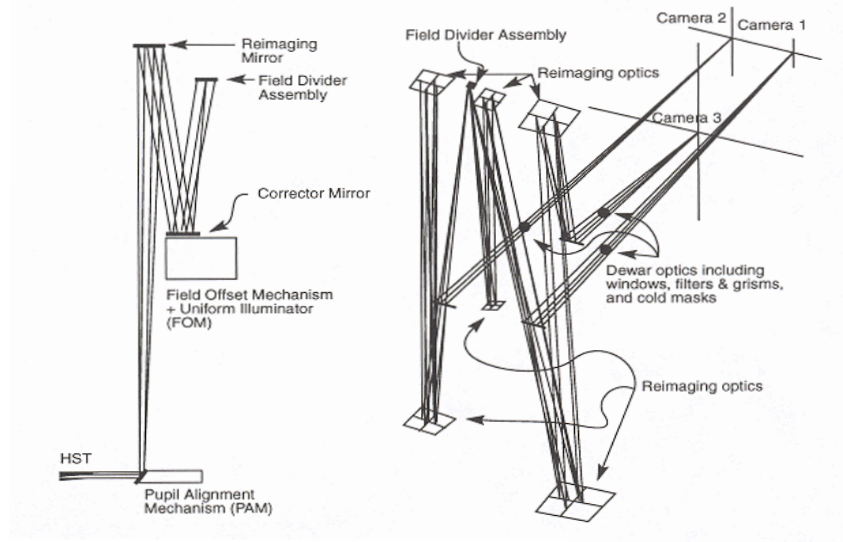
Figure 5: Temperature stability of NICMOS detectors under NCS



The T-1-1 temperature sensor shows that the detectors are stable under operation of the NCS, and do not change by more than 0.1 K on long time scales (see Figure 5), hence variations seen in the thermal background are not directly due to changes in detector sensitivity. We therefore investigated the thermal stability of the NICMOS enclosure and the nearby telescope assembly.

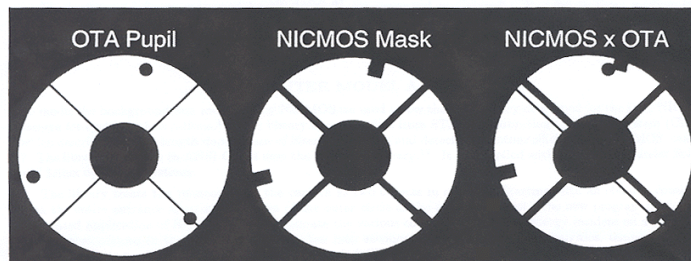
Elements in the NICMOS box which could have a direct affect on the thermal background include the NICMOS fore-optics: the re-imaging mirror (RM), FOM, PAM, filter wheels, dewar window, pupil, baffles, bend mirrors, FDA (imaging mirrors) and cold mask. Only the filters and the cold pupil stop are located inside the dewar. All the other optical elements are warm surfaces. The dewar window is a warm element but does not make any significant contribution to the thermal background. A schematic optical path diagram of the NICMOS fore-optics is presented in Figure 6.

Figure 6: Optical path diagram of the NICMOS fore-optics



The telescope primary and secondary mirrors play significant roles in the thermal background because of their high temperatures (~290K) compared to the detector temperature. In addition, the dewar anomaly in Cycle 7 caused a deformation of the optical bench and an offset of the cold mask. This offset allows the cameras to actually ‘see’ warm parts of the telescope. The cold mask is no longer aligned with the entrance pupil of the telescope and warm portions of the exit pupil which should have been masked by the cold stop are visible (see mask diagram in Figure 7). Modeling from Cycle 7 datasets has shown that the offset is approximately 11% of the pupil radius (see Krist 2000). Proposal 9704 was designed to determine the cold mask offset for NICMOS cameras 1, 2 and 3, and hence provide new parameters for TinyTim. No change in the offset of the cold mask since the end of Cycle 7 was found for Cycle 11(see Roye et al 2003). The cold mask was moving during the early part of Cycle 7 in association with the dewar anomaly, but currently appears stable. This alignment affects the NICMOS PSF and has resulted in a change of the photometric aperture corrections, as modelled by the TinyTim software, this aspect will be discussed in a future photometry ISR.

Figure 7: Representation of cold mask misalignment



A short explanation of sensor locations around NICMOS

Working from the detectors out through the dewar, one can refer to groups of thermal sensors which operate in similar environments. The inner most part of the dewar contains the detectors, dewar window, and filters (See Figure A.1).

The filter wheel housing is inside the dewar, and because of the thermal short is thermally coupled to the cold mask housing.

The Vapor Cooled Shield (VCS) surrounds these items and is encased by two Thermal Electric Cooling shells (TECI/TECO) and finally the main shell of the dewar. Two sets of sensors lay under the TECI and TECO radiators located outside of the main shell of the dewar, but thermally coupled to the TEC shells.

The NDWTMP* sensors are numbered according to their position in the dewar (See Figure A.5). Sensors inside the VCS begin with the value 1. Sensors between the VCS and the TECI shield begin with the value 2. Sensors between the TECI and TECO shields (or thermally coupled to them) begin with a value of 3 and those just inside the main shell begin with a value of 4. The NICMOS fore optics and truss lie outside the main dewar shell, and are at a higher temperature than the detectors.

Table 2 lists the elements that could have a thermal impact on the detectors, and their current range of operating temperatures - measurements were taken over approximately a 200 day period. By referring to Figure A.2 and Figure A.5 it can be seen that sensor readings taken further away from the detector show a wider swing in temperatures over the given time scale, as well as an increased temperature reading in general. This is expected since not all elements in the optical path are inside the cold, stable, operating environment of the dewar and the further out of the dewar one recedes, the more the environment of the telescope plays a larger role.

Table 2. Temperature sensor readings from NICMOS, Cycle 11 and Cycle 7/7n

Keyword	Description	Cycle 7	Average $\Delta C_{11} - C_7$	Cycle 11	Units
NDWTMP21	Camera 2 Cold Mask temp (between detectors and VCS)	100.7	+11.4	112.10	deg K
NDWTMP22	Camera 3 Cold Mask temp (between detectors and VCS)	100.7	+11.4	112.10	deg K
NDWTMP23	Vapor Cooled Shield Forward temp	101.9	+23.5	125.2 - 125.6	deg K
NDWTMP24	Vapor Cooled Shield AFT temp	101.8	+11	112.61 - 112.95	deg K
NDWTMP25	Vapor Cooled Shield MID temp	101.3	+11.3	112.46 - 112.75	deg K
NDWTMP31	Thermoelectric Cooler Inner 1 Base temp (Close to TECI Radiator 1, thermally coupled to TECI Inner Shield)	188.3 - 190.1	+4	193.88- 194.04	deg K
NDWTMP41	Thermoelectric Cooler Outer 1 Base temp (Close to Dewar Main Shell)	215-17	+5	221.308 - 223.626	deg K
NDOSFTMP	Dewar Outer Shell Fore Temp	-9.21 - -5.33	+6.05	-3.395 - 0.970	deg C
NDOSATMP	Dewar Outer Shell Aft Temp	-2.91 - 0.97	+4.37	3.395 - 7.275	deg C
NFOB1TMP	Fore Optical Bracket 1 Temp (Closest to the entrance baffle)	-7.27 - -3.39	+5.33	-1.94 - 1.94	deg C
NFOB2TMP	Fore Optical Bracket 2 Temp (Closest to the FOM, PAM and RM mirrors)	-7.76 - -3.88	+5.34	-2.42 - 1.46	deg C
NFORBTMP	NICMOS Fore Bulkhead Temp (front of the NICMOS enclosure)	1.46 - 4.36	+3.39	4.36 - 8.24	deg C
NAFTBTMP	NICMOS Aft Bulkhead Temp (Rear of NICMOS enclosure)	6.31 - 10.67	+8.97	15.03 - 19.88	deg C
NTRS2TMP	Truss 2 Temp	-4.36 - -0.48	+6.06	1.94 - 5.33	deg C
NTRS3TMP	Truss 3 Temp	-0.48 - 2.91	+6.3	5.82 - 9.21	deg C

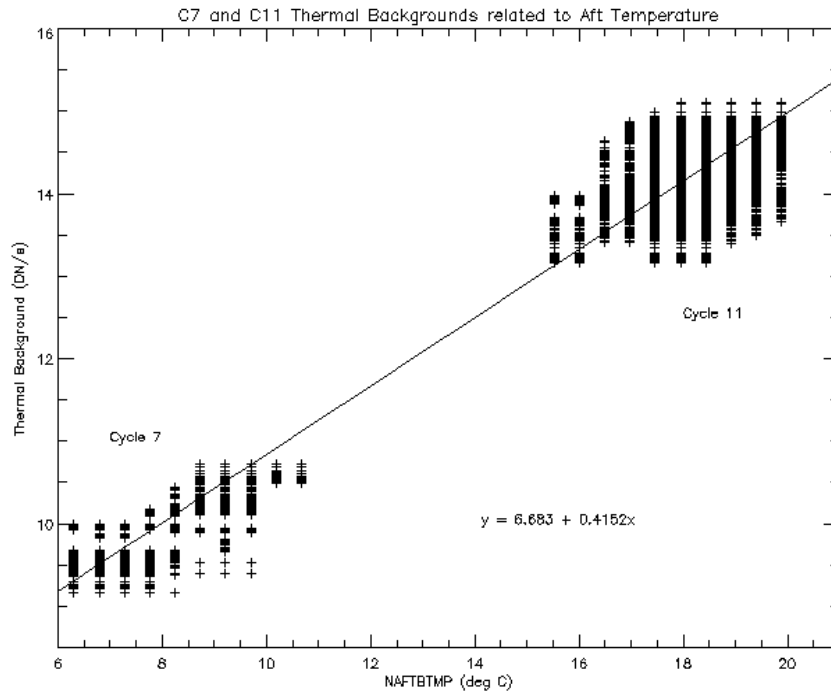
Keywords marked in boldface are those sensors which were found to correlate well with the thermal background measurements taken in both Cycle 11 and Cycles 7/7N

The most anomalous readings come from the VCS sensors. During Cycle 7/7n all three sensors maintained roughly the same temperature reading, but data from Cycle 11 shows that the fore end of the VCS is operating much warmer than the aft end. This can be

explained by the presence of the cryocooler - its coolant lines are connected to the back end of the dewar, creating a temperature gradient of approximately 12 K across the VCS.

Figure 8 plots the aft NICMOS temperature versus the measured thermal background for both cycles. The large spread in y-values is due to the sampling of the available aft temperature data. Both datasets suggest the link between increasing aft temperature and thermal background measurements.

Figure 8: Measured Thermal Background vs. Nicmos Aft Temperatures



Analyzing the telescope thermal environment

Overall, the telescope aft shroud has increased approximately 10K since Cycle 7/7n. There are multiple thermistor sensors (thermally sensitive resistors) in the aft shroud of the telescope which are used to monitor temperature. There are 6 temperature monitors on the MLI blanket outer surface facing the science instruments and OTA. The first 4 monitors are on the cylindrical section and the last 2 monitors are of the aft bulkhead MLI outermost layer. The TAFTBULK temperature reading is a weighted average of all the internal thermal sensors located on the aft bulkhead. There are many sensors which are combined to produce the TASINAFB effective sink measurement, and they include the sensors from the TAFTBULK calculation - so there should be some similarity between the graphs (see Figure 10). Figure 9 shows how the thermal environment of the telescope aft shroud changed between January 1, 2001 and December 30, 2002. The most interesting features of both graphs are the increase in temperature directly after SM3B (during which ACS and

NCS were installed) and the increase in scatter between pre-servicing mission and post-servicing mission measurements in the TASINAFB calculation. No known cause exists for the increase in scatter for the post-SM3B dataset. The sharp change in slope is most likely due to the additional heat load created by the installation of ACS and NCS.

Figure 9: Thermal environment of the HST Aft Shroud around NICMOS 2001 - 2002

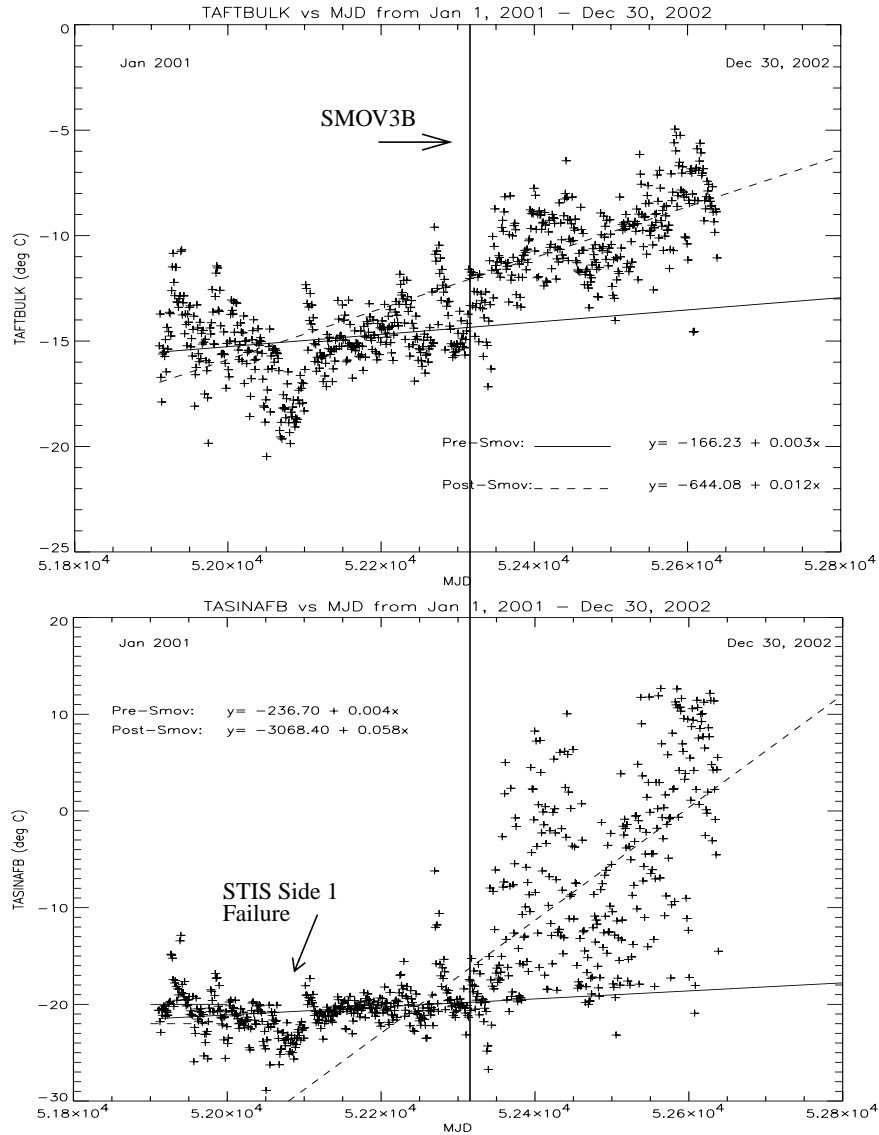
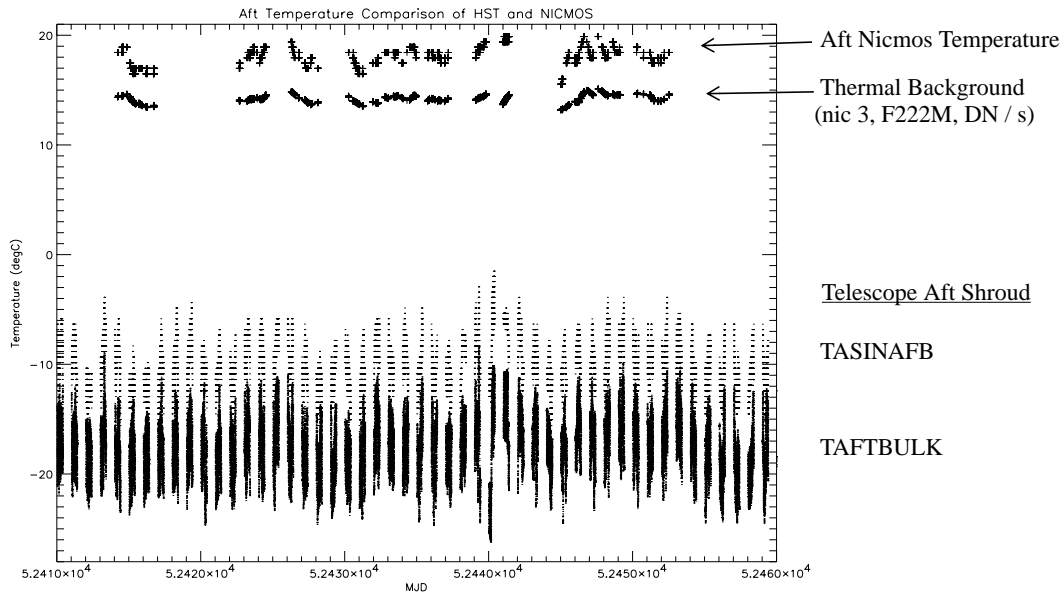


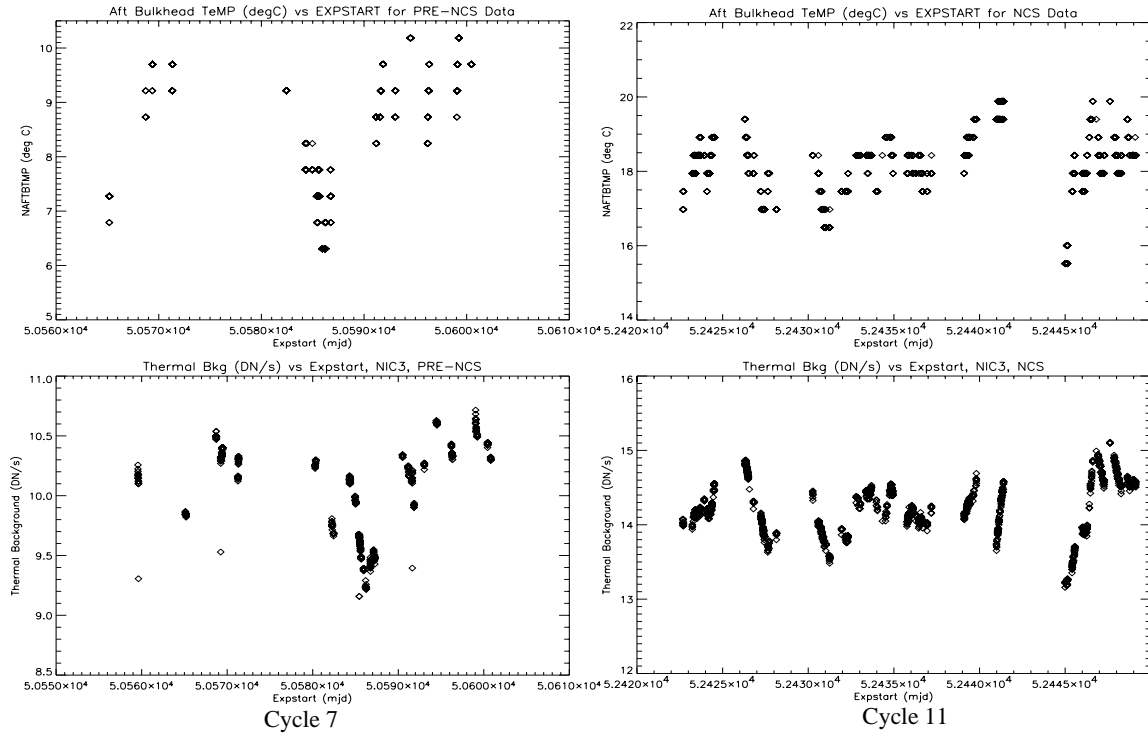
Figure 10: Comparison plot of telescope aft shroud temperature fluctuations with the measured thermal background in camera 3 and the temperature at the aft end of the NICMOS enclosure.



A plot of the thermal background count-rate versus time for both cycles (see Figure 11) shows that a change of 2 K in the aft end of the NICMOS enclosure roughly translates to a change of 1 DN/s in the detected thermal background. Similar trends can be seen in other temperature sensors located outside the main dewar and they are similar for all cycles. This infers that the variation seen in thermal background is not due merely to the addition of the NCS, but the thermal environment of the telescope as a whole (as expected). The sampling between the NAFTBTMP keyword and the thermal background differs because the aft sensor is only sampled once every minute.

In Cycle 7, the average thermal background in camera 3 F222M was 10.06 DN/s, with average aft temperature in the NICMOS enclosure (NAFTBTMP) of 8.5C. In Cycle 11 the thermal background for the same combination was 14.18 DN/s, with an average aft temperature of 17.5C, a change of approximately 9C. However, there is a temperature gradient across the enclosure, the fore-optics swing in temperature in the same manner as the aft end of the enclosure, but with a smaller amplitude.

Figure 11: Comparison of thermal background measurements to the temperature at the aft end of the NICMOS enclosure (taken from NAFTBTMP) for all cycles.



A plot of the second fore-optical bracket sensor reading (which gives the closest estimate for the temperature of the fore optics) indicates that a 2K variation in temperature translates to a 1.5 DN/s change in the thermal background - in the same direction as the temperature swing (Figure 13). Comparing the change in temperature of the fore-optics from Cycle 7 to Cycle 11 this leads to the conclusion that the increase of 5 degrees should yield an increase of about 3 DN/s in thermal background - which closes the gap between the additional signal that was measured in the on-orbit datasets and the predicted change in DQE! This is supported by a simple model of thermal background emission from the fore-optics.

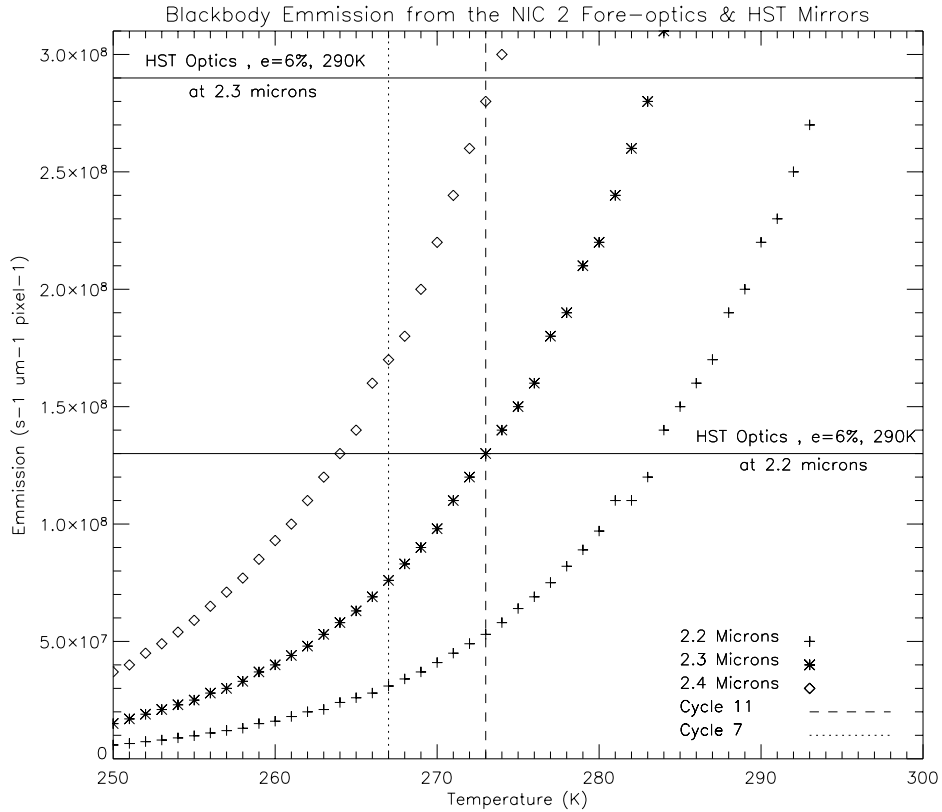
Figure 12 is a simple blackbody comparison of the HST primary and secondary optics with the NICMOS fore-optics (using NIC2 optical parameters). The model takes into account blackbody emission at the specified wavelength (the central wavelength of the filter of interest for example), a given temperature, the solid angle subtended on the sky (for pixel scale) and an emissivity. This follows the general form:

$$\text{thermal emission}_{2.2\mu} = A\omega B(\lambda, T_K) e_{2.2\mu}$$

Where A is the area of the entrance pupil and ω is the solid angle of the detector as project by the optical system on the sky. The HST optics have remained thermally stable since cycle 7 and have a combined emissivity of approximately 6%. The NICMOS fore-optics have changed temperature, by an average estimated 5K between cycles, and they

have a combined emissivity of approximately 10%. These values were used to derive the thermal emission models represented in Figure 12.

Figure 12: Simple blackbody comparison of HST and NICMOS optical surfaces, using NIC 2 optical parameters



By referring to Figure 12 and doing some simple math, one can estimate an increase of 14% in the emission seen from the NICMOS fore-optics, which is non-negligible when compared with the HST optics. This is further supported by the complete thermal background estimate calculated by the full NICMOS ETC thermal background code.

	2.2μm emission [s ⁻¹ / μm ⁻¹ / pixel ⁻¹]	HST 2.2μm emission [s ⁻¹ / μm ⁻¹ / pixel ⁻¹]	Ratio
Cycle 7	3.1e7	1.3e8	24%
Cycle 11	4.9e7	1.3e8	38%

In general, the peak radiation has shifted a small amount towards the red, which is consistent with Wien's Law for the warm optics that the NICMOS cameras see. The largest change can be seen in the cold mask, where the peak emission has shifted approximately 3 microns, corresponding to a change in emitted energy of ~ 54% (over all wavelengths). However, the peak emission is still in the long mid-IR region, so the total change in emis-

sion at near-IR wavelengths is still small - inferring that the contribution from the hotter cold mask probably hasn't changed much from Cycle 7.

Figure 13: Fore-Optical Bench and Truss Temperature sensor variations in Cycle 11

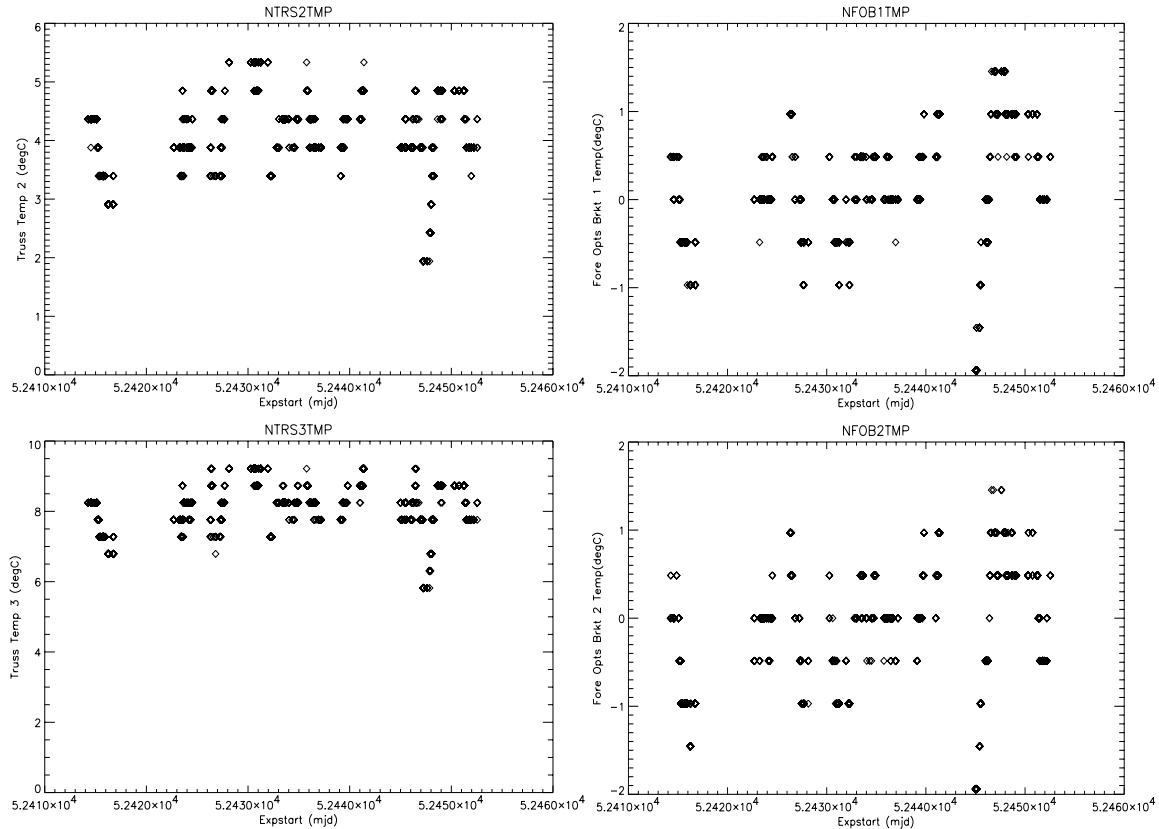


Figure 13 illustrates the temperature variation seen across the instrument as it's heated by the aft shroud. The truss 3 sensor (NTRS3TMP) is located at the aft end of the truss, and the truss 2 sensor (NTRS2TMP) much closer to the fore- end - the average temperature difference between these sensors is 4 C.

ETC Software and Predictions for the thermal background

The NICMOS ETC software includes a thermal background library which estimates the amount of observed thermal background for any given exposure (based on the users input parameters). The library was originally developed in C (Sivaramakrishnan 2000), but has recently been added to the Synphot package in IRAF for easy maintenance and integration into the APT user tools.

Knowing the étendue, reflectance, emissivity and temperature of each of the optics allows the code to estimate the total thermal contribution to the exposure. Etendue is the product of the area of the optic and the solid angle of the detector on the sky. The entrance pupil area for NICMOS is the HST primary's visible area as seen from the detector. To check that the ETC reflected the same increased thermal emission estimates from hotter fore-optics, updated reference tables were created and run through a test version of the

Synphot code. The results showed that the measured increase in the cold mask temperature had negligible effect on the estimated thermal background. However, the combined increases of all the optical elements can well account for the increase in observed background. Table 3, which lists the parameters for each of the elements in the optical train, is useful for identifying which elements have the most ‘weight’ for estimating a thermal background.

Table 3. Optical path elements associated with the thermal background model

Optical Element	Type	Emissivity	Beamfill ^a	Avg. Temp(K) Cycle 7	Avg. Temp(K) Cycle 11	Source
(FOM) pupil	Thru	0.0349	0.74	267	270	sensor
primary mirror	Thru	0.03	0.67108	288 ^b	290	CCS-Lite ^c
secondary mirror	Thru	0.03	1.0	290 ^b	290	CCS-Lite
dewar window	Thru	0.05	0.74	60	77	
(PAM) bend1	Thru	0.058	0.74	267	270	sensor
bend2	Thru	0.058	0.74	270	-	-
imaging mirror	Thru	0.058	0.74	270	271	-
parabolic 1 ^d	Thru	0.058	0.74	270	271	-
parabolic 2 ^d	Thru	0.058	0.74	270	-	-
reimaging mirror	Thru	0.058	0.74	267	270	sensor
cold mask	Thru	0.15	0.2499	100	112	sensor
coronagraphic hole	Opaque	0.95	0.0104	272.6	-	-
edge baffle	Opaque	1.0	0.0354	253	-	CCS-Lite
pads	Opaque	1.0	0.01	288	288	CCS-Lite
spider	Opaque	1.0	0.049	256	256	CCS-Lite

a. Beamfill is a derived scaling factor used for optics which have multiple surfaces at different temperatures and emissivities (ex: the primary mirror with pad, spiders etc). In these cases the Plank function is weighted by the filling factor of the area that optic contributes to the thermal background.

b. Temperature taken from Roberto et al

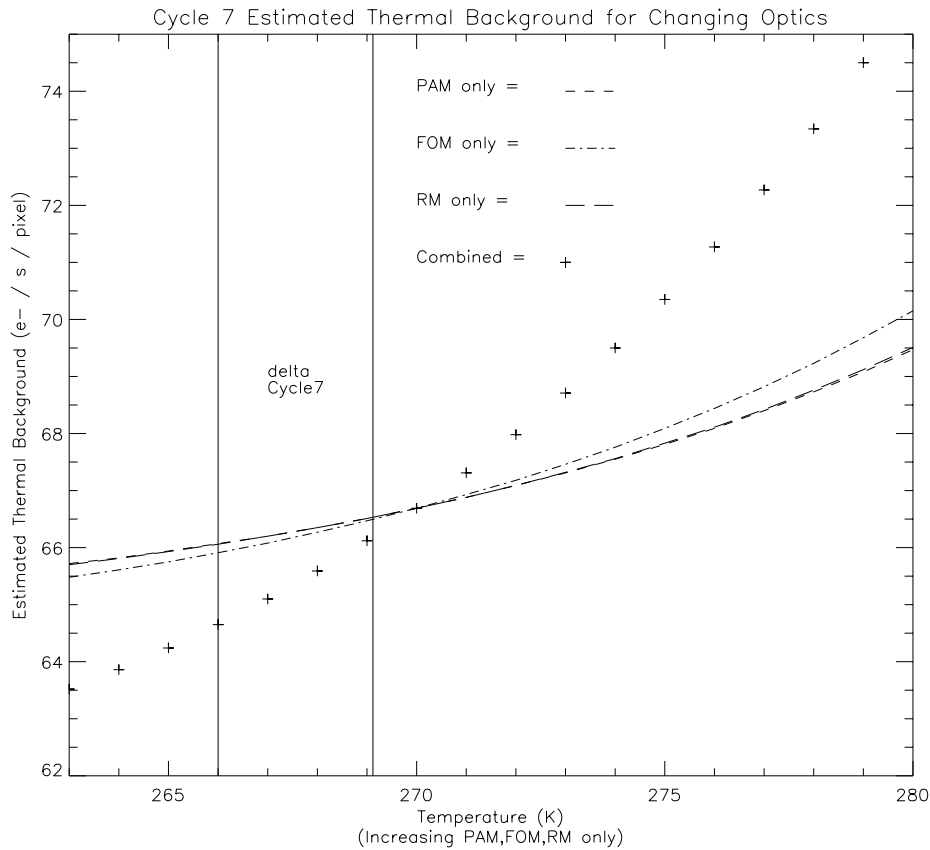
c. CCS-Lite is a web interface to the HST controlling monitors, it contains sensor information which is frequently updated.

d. These are reimaging mirrors which enable the three plate scales at f/17, f/44 and f/80 in nic[123].

Figure 14 is a graph of the estimated thermal background resulting from changing the temperatures of several of the NICMOS fore-optic elements. For these cases the temperature for the FOM, PAM and reimaging mirror were changed independently - keeping all other optics at stable temperatures. Then, all three of these optics were varied at the same time. The resulting thermal background estimates are plotted against the applied

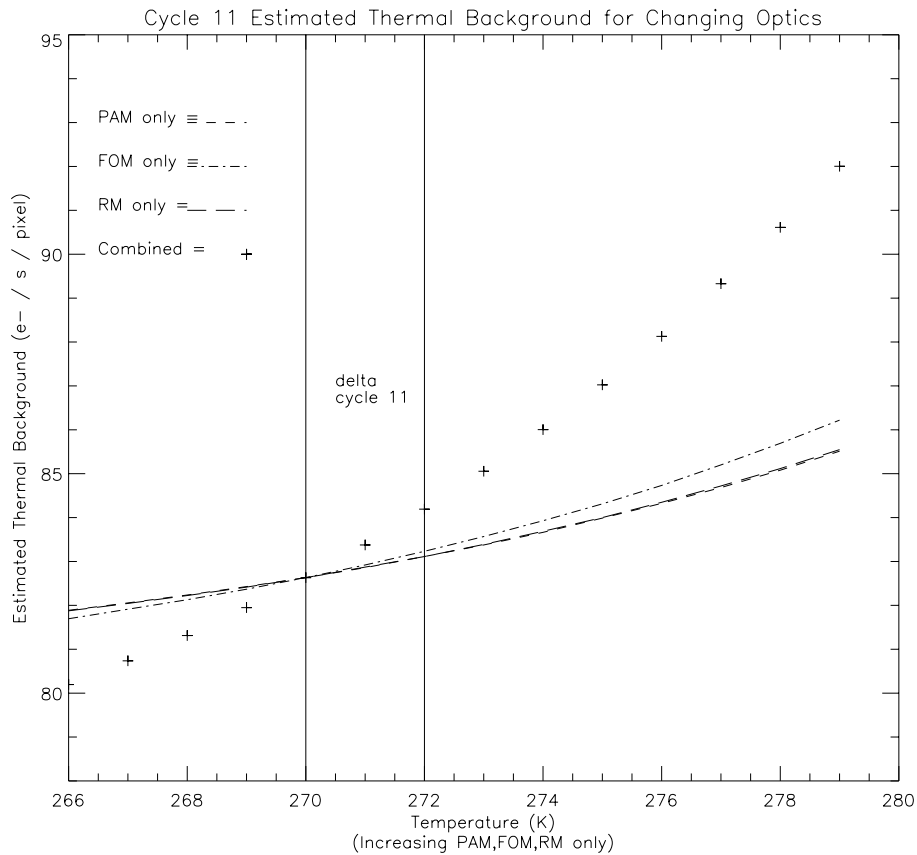
temperature. The temperature range was derived from the NFOB2TMP keyword which is mounted to the fore optical bracket which contains these elements (see Table 2).

Figure 14: Cycle 7 Estimated thermal background emission from fore-optics



The same was done for the Cycle 11 data, those results are shown in Figure 15. At first glance one may think it odd that points modeling all three optics at the same temperature (+) start much lower than the individual optic models, however, the individual models were created by changing only the one specified optic temperature, hence the others were all at the higher median temperature for that cycles data, giving a larger total background estimate. For Cycle 11 the median temperature measured from the fore optics bracket was 271K. For Cycle 7 the median temperate was 267K. Figure 15 shows that an estimated 3 e-/s/pixel change in the thermal background could be observed over the measured temperature range of the optical elements - and indeed, this is seen in the thermal background observations. Test cases run through the ETC as well as just the thermal background portions of the code are typically accurate to within 5-10% of the observed value.

Figure 15: Cycle 11 Estimated thermal background emission from fore-optics



Conclusions

The overall temperature environment of NICMOS and the operating temperature of the detectors has changed since initial operation in Cycle 7. These changes include the following:

- an increased detector operating temperature of ~ 77.1K, from 60K in Cycle 7
- an increase in temperature of the aft end of HST in general
- an increase in temperature of the aft end of the NICMOS enclosure and the NICMOS fore-optical bench
- an increase in the observed thermal background in camera 2 and 3, dependent on wavelength. Approximately half of this increase is accounted for by the improved DQE of the detectors while the rest may be accounted for by the changing temperatures of the NICMOS fore-optics.

These temperature increases affect cameras 2 and 3 in filters whose central wavelength is longward of 2 microns, with the exceptions of the F175W filter in camera 3 which has a bandwidth covering ~ 1.2 - 2.3 microns. Both the F175W and F240M filters in camera 3 have much higher thermal background than the F222M filter, which should be taken into account for any observational planning. Camera 1 does not contain any such filters and hence was not considered in this analysis, and should not impose any thermal background limitations.

Thermal background measured at the detectors can be variable on time scales of a day. The largest variations are seen in long wavelength, camera 3 observations, but should not significantly impact any science for that filter (other than F240M which has always shown high levels of thermal background). Camera 2 is also affected but shows smaller amplitude variations as well as a lower level of thermal background radiation in general, per pixel. When the thermal background data is scaled such that the camera 2 data represent the same area/pixel subtended on the sky as the camera 3 data, these differences become negligible.

Trends seen from the HST aft shroud temperature plots indicate that the average temperature inside the telescope will continue to increase - this was predicted and is not an unexpected result. The addition of the Aft Shroud Cooling System in a future servicing mission may help reduce the effect of higher temperatures on NICMOS, assuming that it both cools the aft shroud environment and does not create an additional heat load on the NCS radiators. Users should include thermal background images for all exposures planned in filters longward of 1.9 microns so that the background can be appropriately subtracted from the science images. At longer integration times users are most likely interested in detection signals, with typically low signal-to-noise ratios. An increased thermal background will mean that pixels will saturate sooner and a shorter exposure time may be needed (but can be compensated for by taking more exposures), this should have no significant impact on science in the affected long wavelength filters.

References

Daou, D. and Skinner, C., NICMOS-ISR-97-025

Daou, D. and Calzetti, D., NICMOS-ISR-98-010

Krist, J. E. and Golimowski, D. A. and Schroeder, D. and Henry, T. J., PASP, v110, pp.1046-1058, 2000

Krist, J. E., NICMOS-ISR-99-011

Robberto, M. et al, Proc. SPIE v4013, p. 386-393

Roye, E. et al, NICMOS-ISR-2003-004

Sivaramakrishnan, A. et al, NICMOS-ISR-00-001

Instrument Science Report NICMOS 2003-007

Sivaramakrishnan, A. et al, NICMOS-ISR-200-005

Sosey, M. NICMOS-ISR-2001-001

Strecker, D., SER SYS-062

Appendix A

Useful diagrams of the NICMOS enclosure and surrounding Telescope environment.

Figure A.1: Dewar Configuration

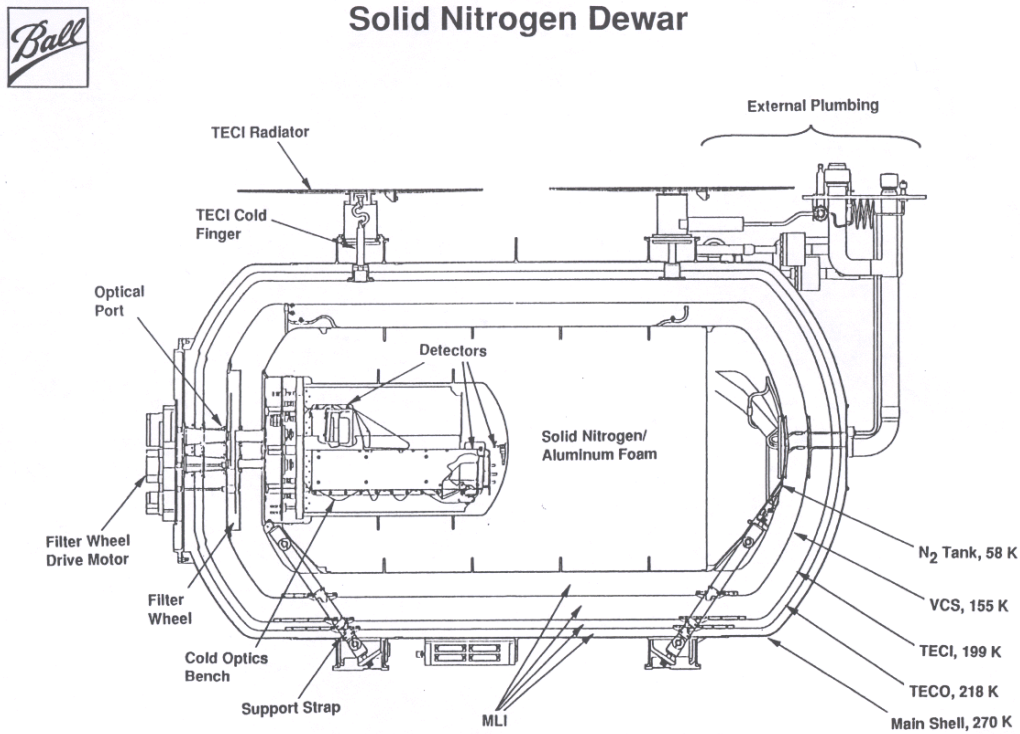


Figure A.2: NICMOS Exterior Sensor Locations

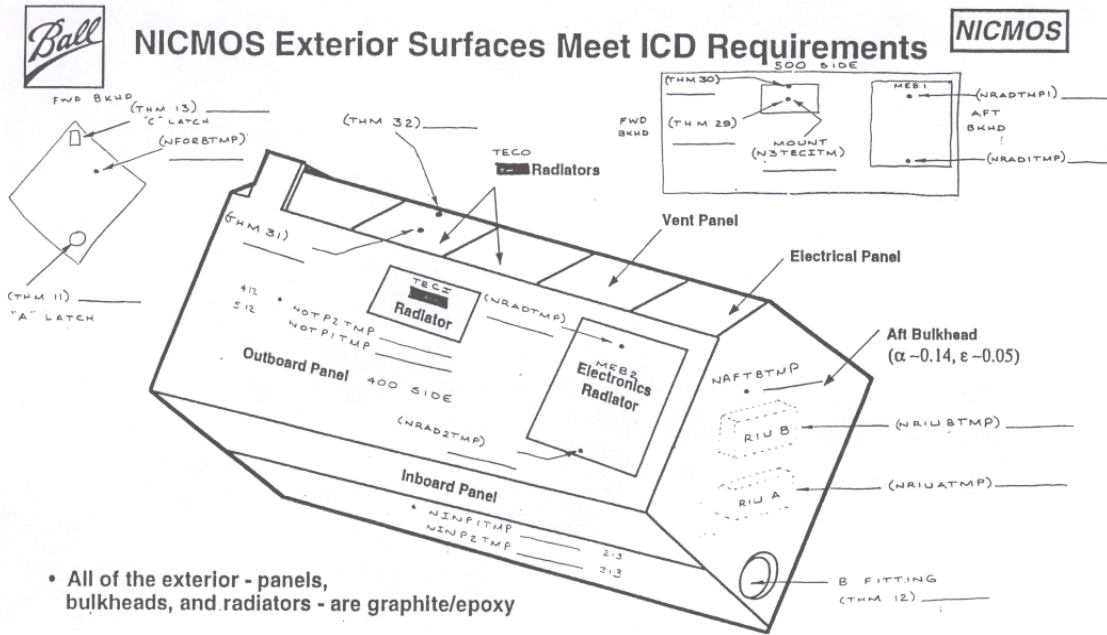


Figure A.3: Fore-Optics support and sensor locations

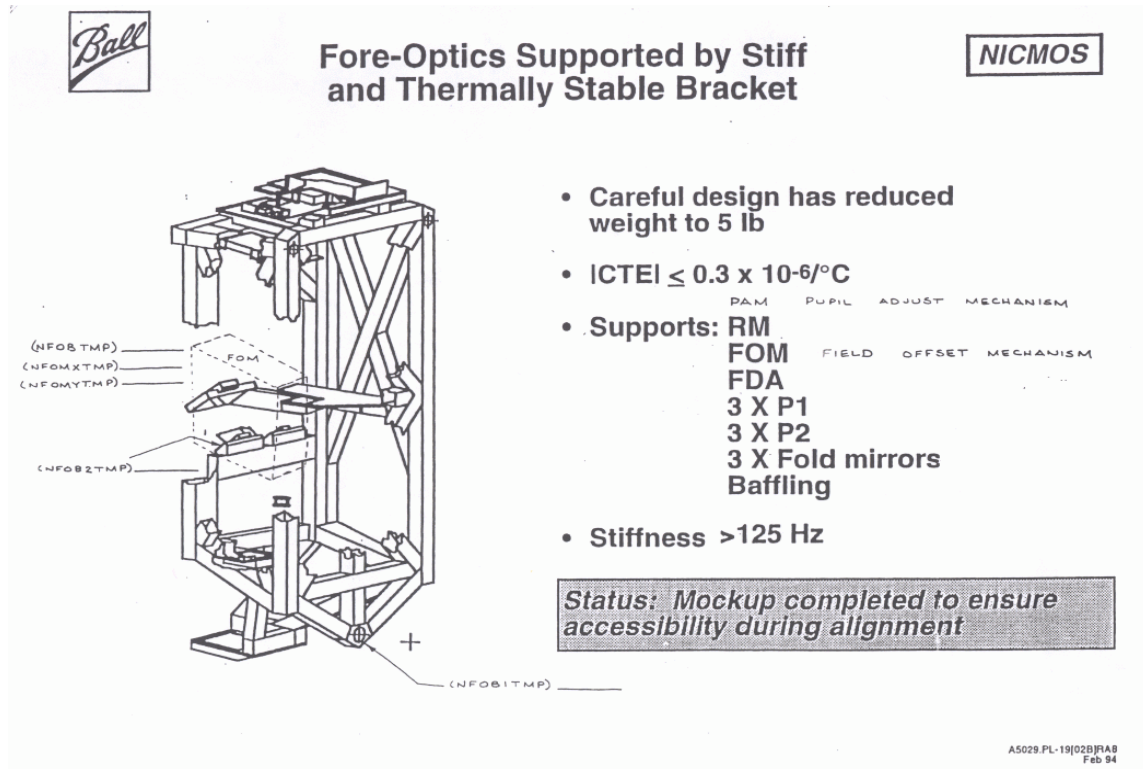


Figure A.4: NICMOS coolant plumbing - the NCS coolant lines are attached to the aft end of the NICMOS enclosure - through the Sealing Cap and to the Capillary Line.

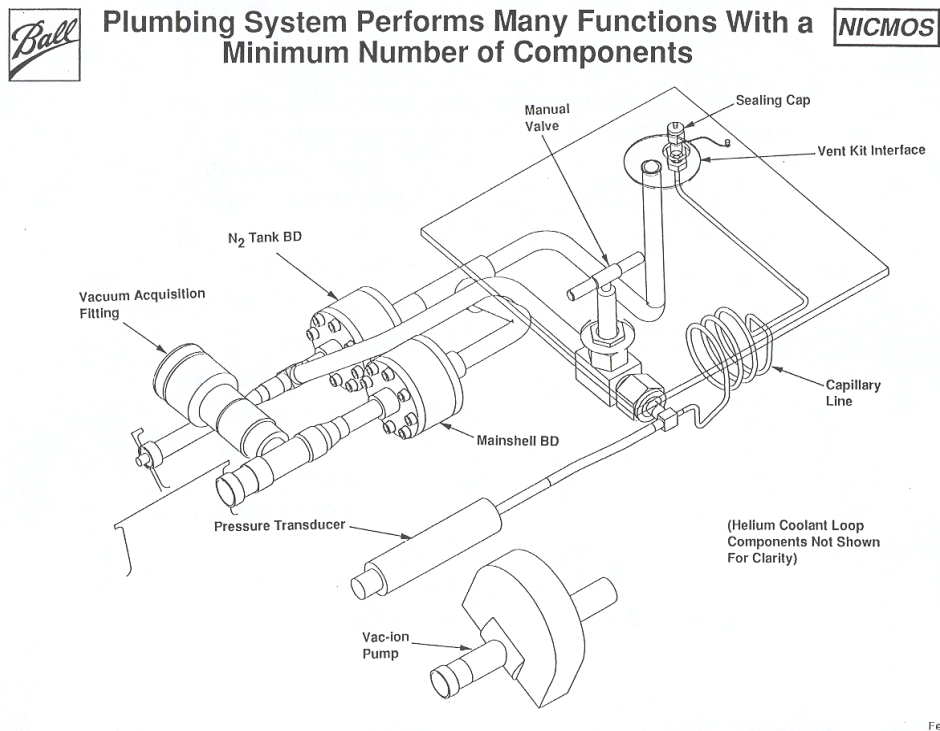


Figure A.5: Dewar Temperature Sensor Locations

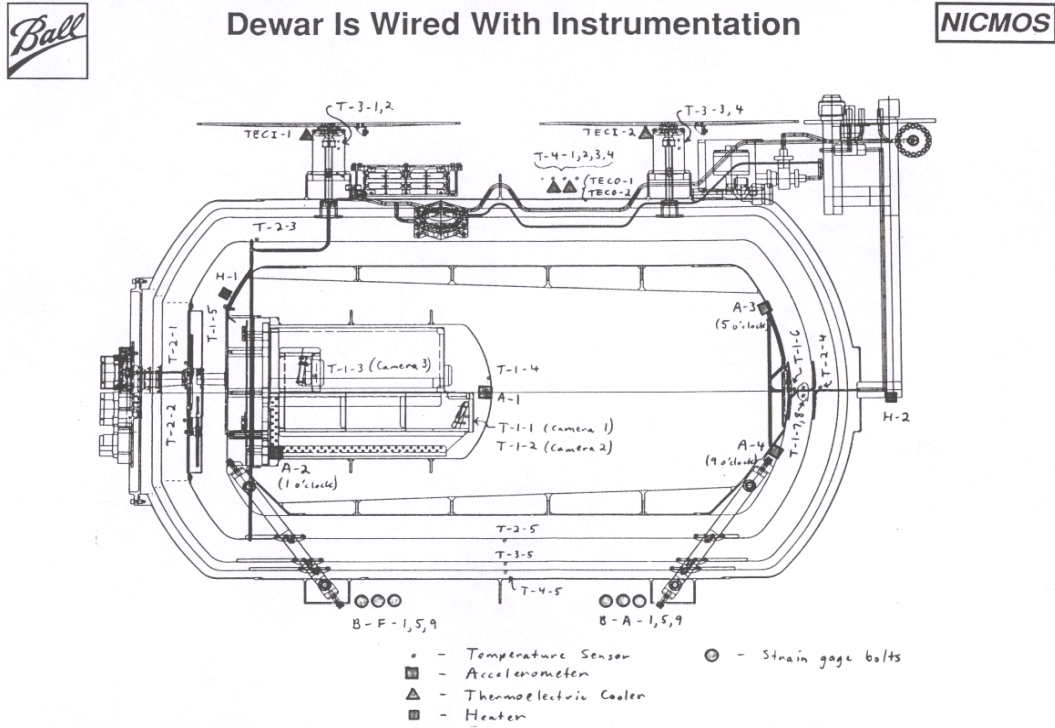


Figure A.6: Shield Configuration Cut-out

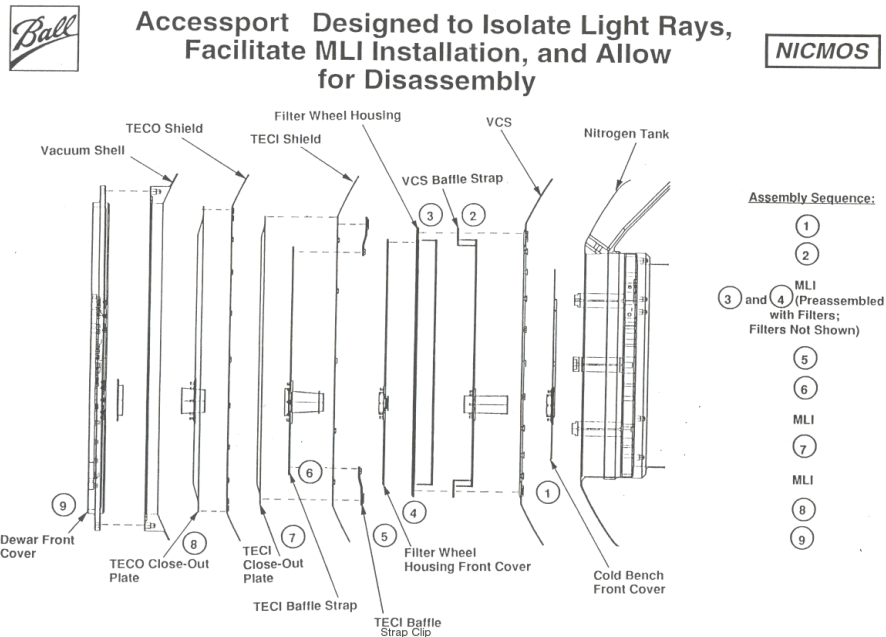


Figure A.7: NICMOS enclosure showing external temperature sensor locations

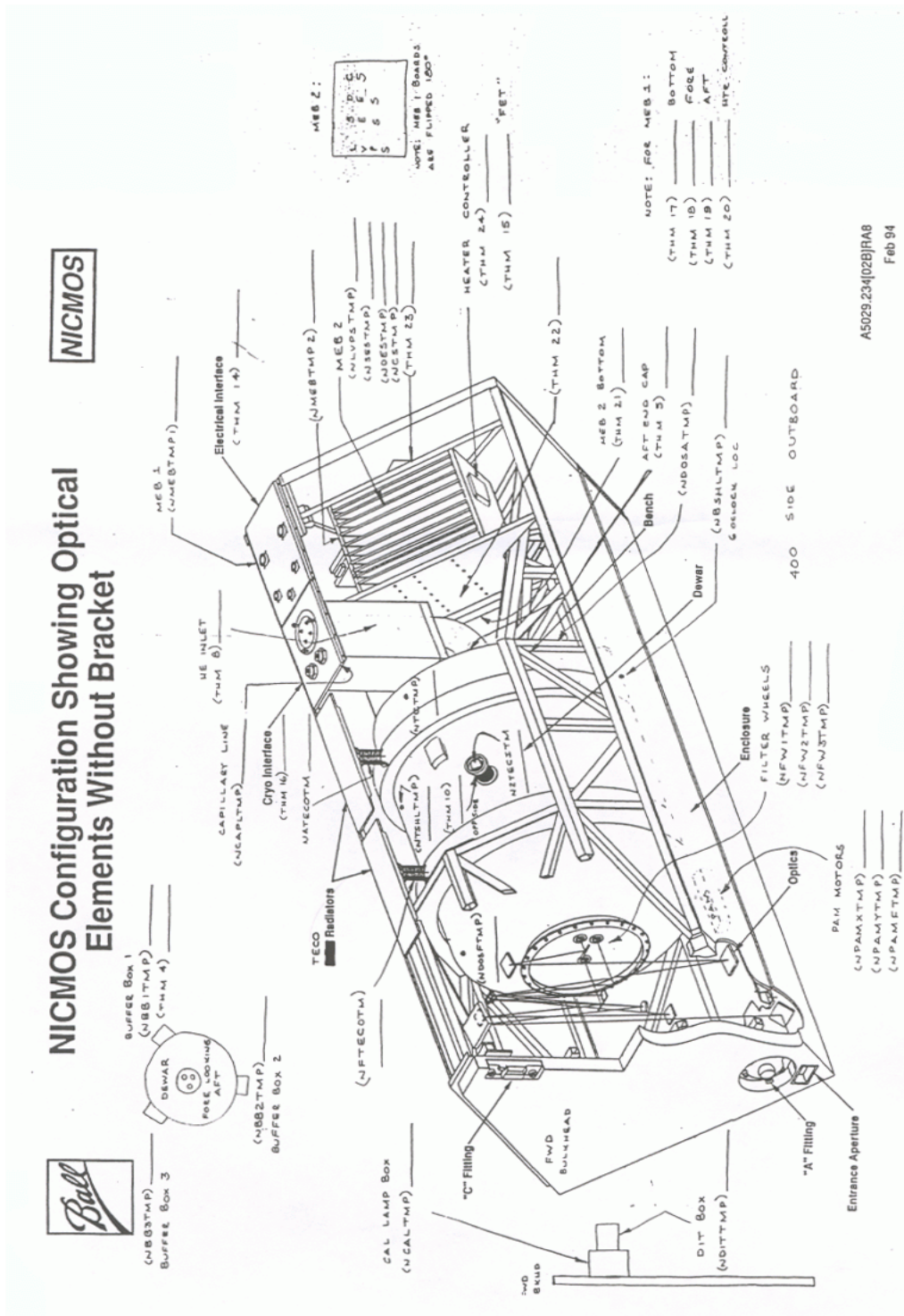


Figure A.8: NCS location on HST. (ASCS not yet installed on HST)

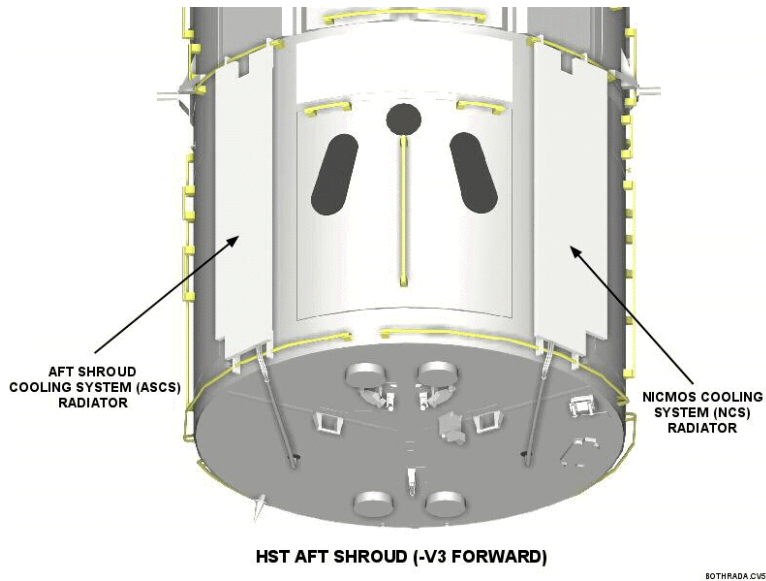
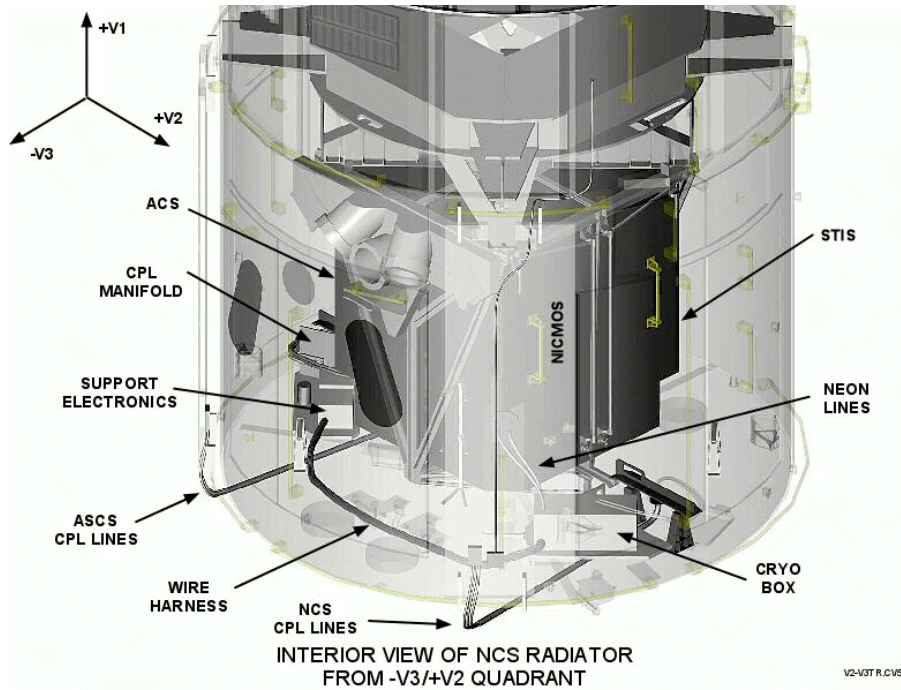


Figure A.9: Overview of instrumentation locations on HST

